Supplementary Information

A universal ligand mediated method for large scale synthesis of transition metal single atom catalysts

Yang et al.

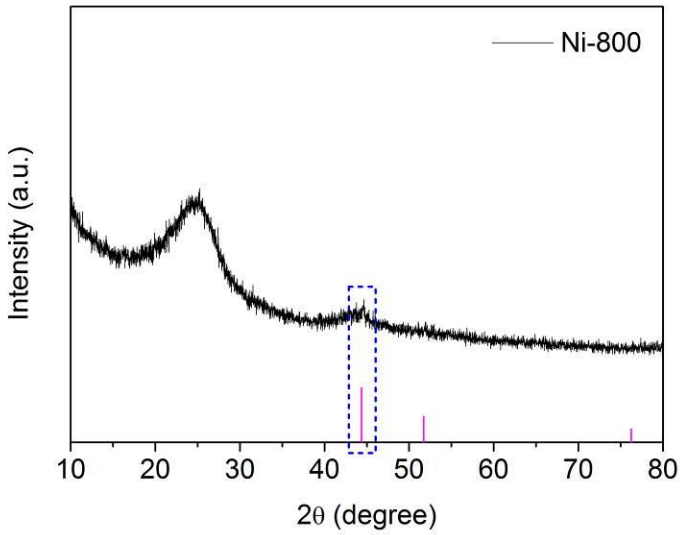

Supplementary Figure 1 | Characterization of the Ni precursor following pyrolysis at 800 ºC. XRD pattern for Ni-800.

Supplementary Figure 1 confirmed that some Ni clusters were formed when the Ni precursor was pyrolyzed at 800 ºC. Clearly at such temperatures, Ni atoms have sufficient mobility to aggregate into small clusters and nanoparticles.

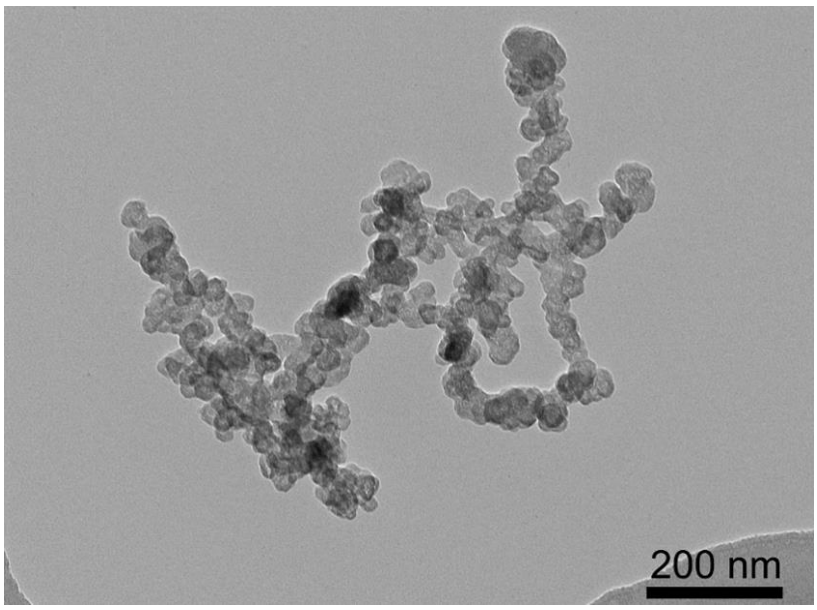

Supplementary Figure 2 | Morphology of Cr-SAC. TEM image of Cr-SAC.

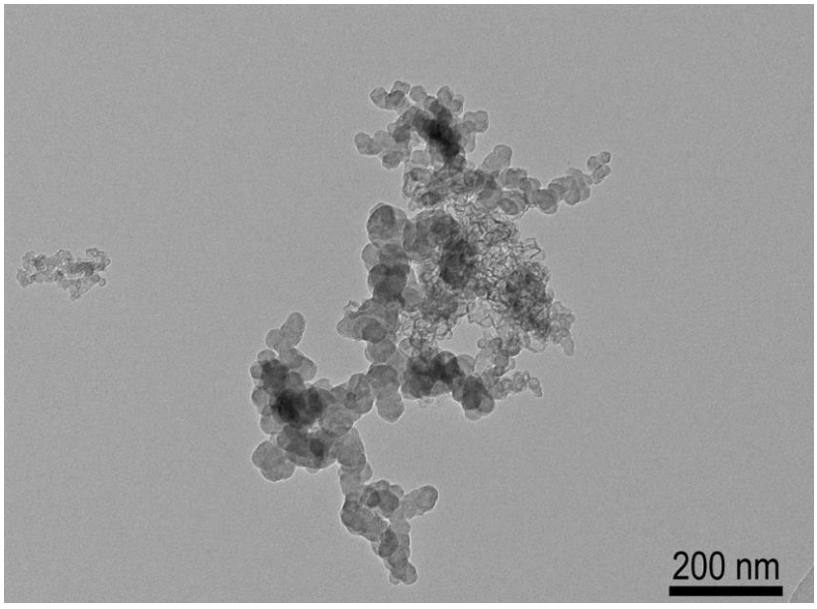

Supplementary Figure 3 | Morphology of Mn-SAC. TEM image of Mn-SAC.

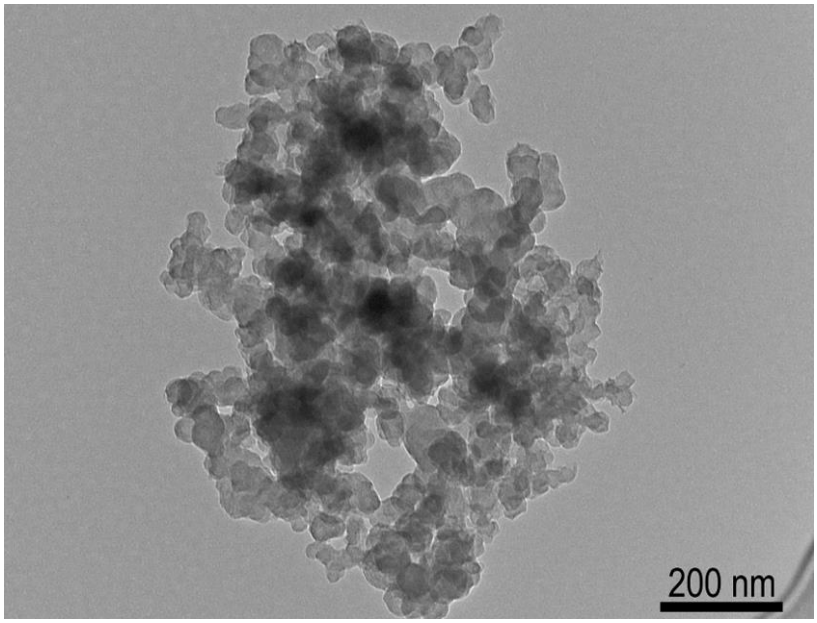

Supplementary Figure 4 | Morphology of Fe-SAC. TEM image of Fe-SAC.

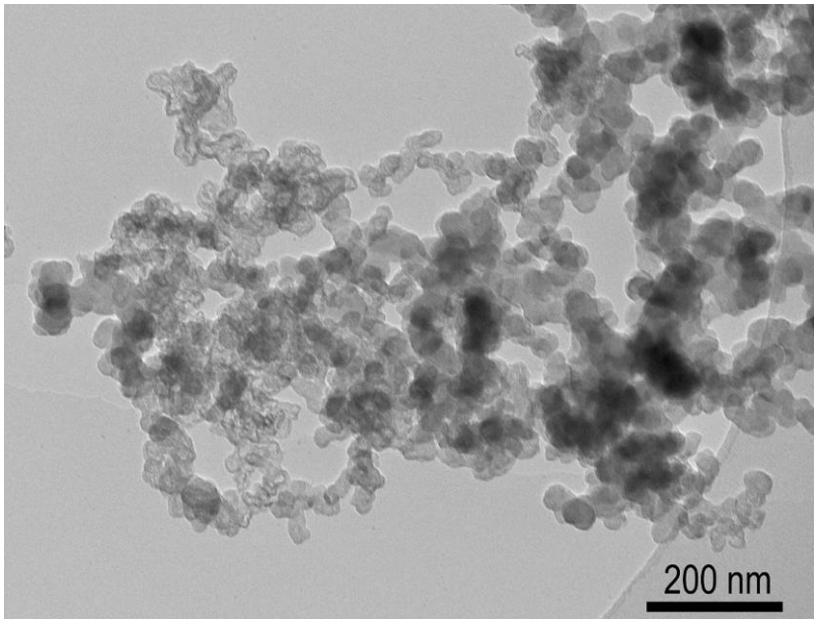

Supplementary Figure 5 | Morphology of Co-SAC. TEM image of Co-SAC.

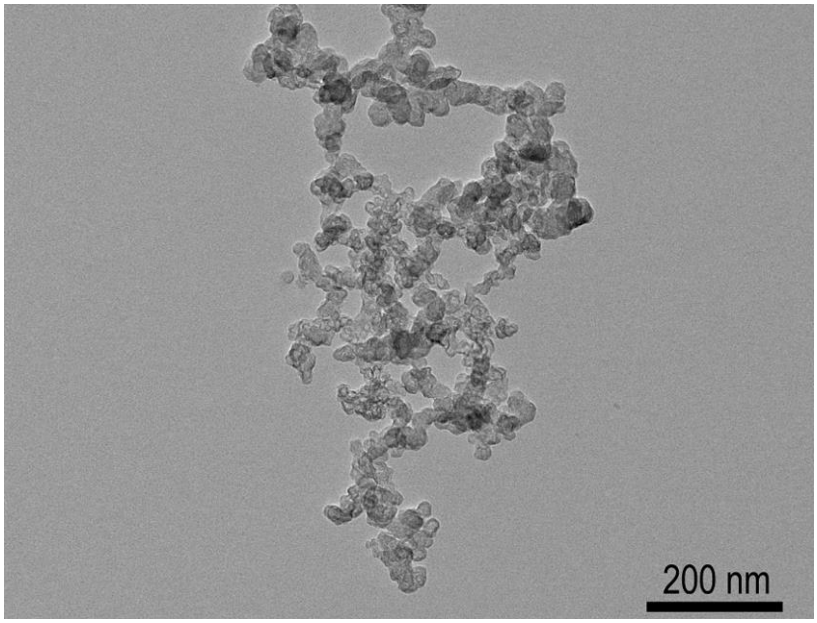

Supplementary Figure 6 | Morphology of Cu-SAC. TEM image of Cu-SAC.

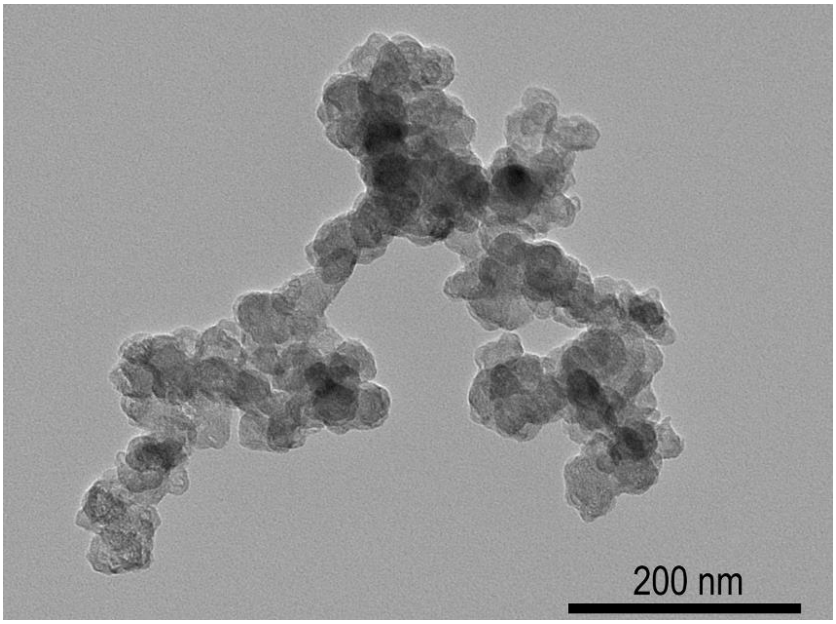

Supplementary Figure 7 | Morphology of Zn-SAC. TEM image of Zn-SAC.

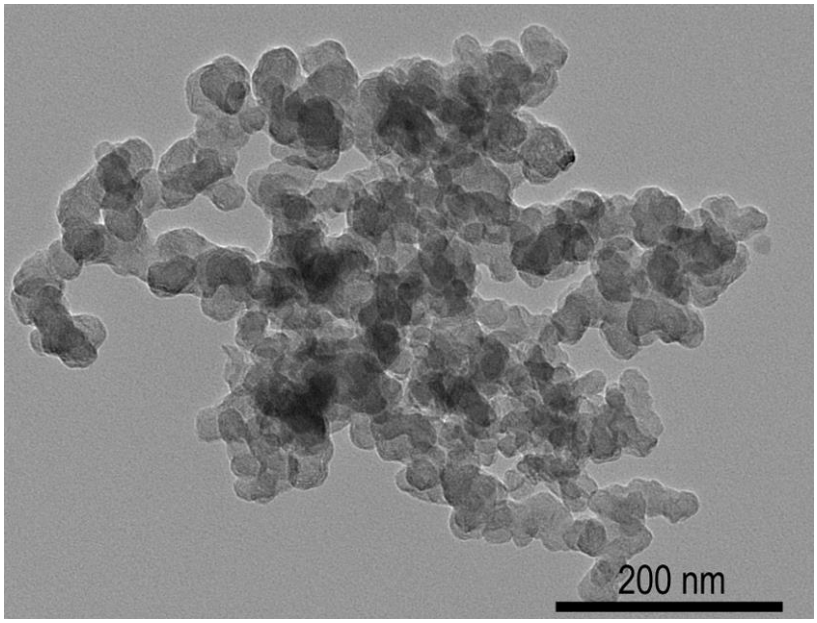

Supplementary Figure 8 | Morphology of Ru-SAC. TEM image of Ru-SAC.

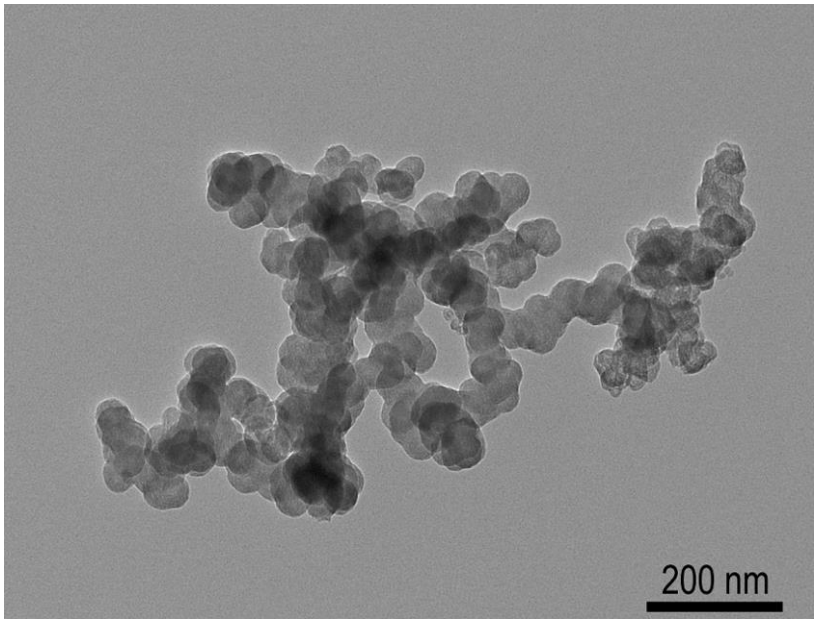

Supplementary Figure 9 | Morphology of Pt-SAC. TEM image of Pt-SAC.

Supplementary Figures 2-9 confirm that all M-SACs possessed the structure of carbon black. No metal nanoparticles were observed for any of the M-SACs, indicating that metal atoms in these materials were highly dispersed.

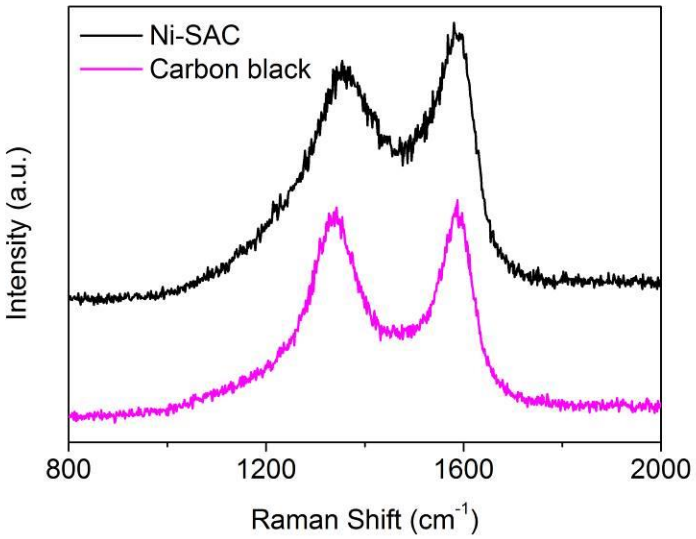

Supplementary Figure 10 | Characterization of Ni-SAC and carbon black. Raman spectra for Ni-SAC and carbon black.

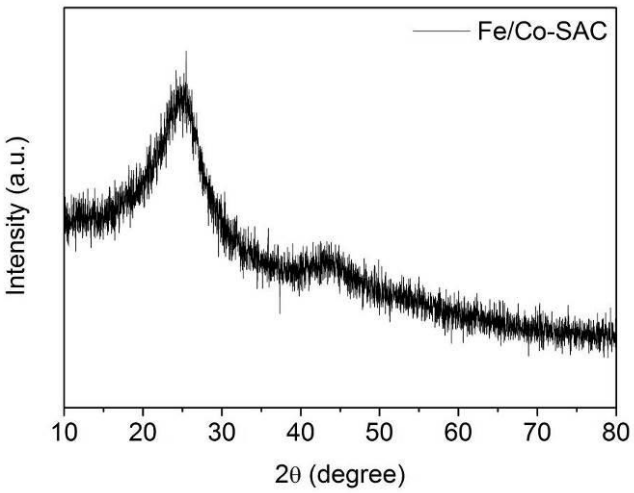

Supplementary Figure 11 | Characterization of a bimetallic SAC. XRD pattern for Fe/Co-SAC.

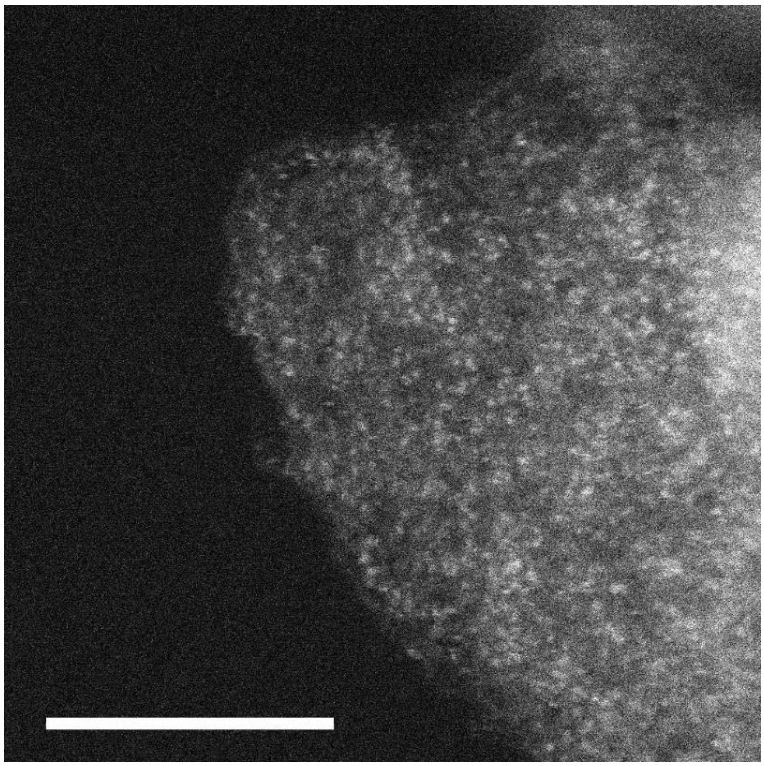

Supplementary Figure 12 | Morphology of a bimetallic SAC. HAADF-STEM image for a Fe/Co-SAC, scale bar: 5 nm.

Supplementary Figure 12 confirms that the Fe and Co were atomically dispersed in Fe/Co-SAC.

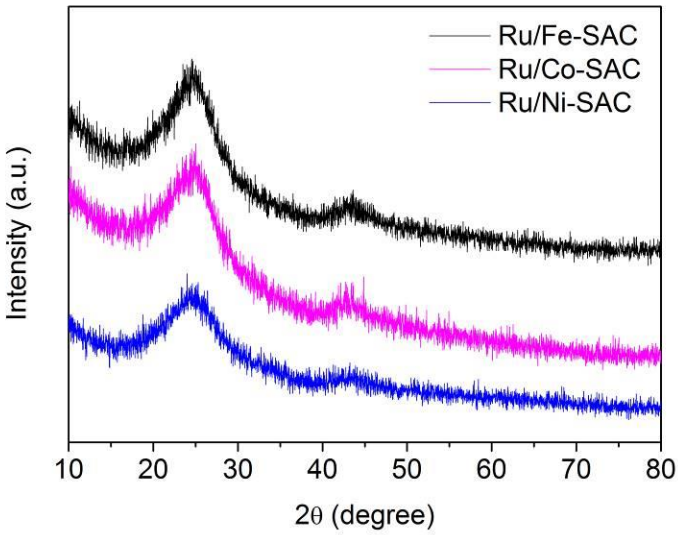

Supplementary Figure 13 | Characterization of bimetallic SACs. XRD patterns for Ru/Fe-SAC, Ru/Co-SAC, and Ru/Ni-SAC.

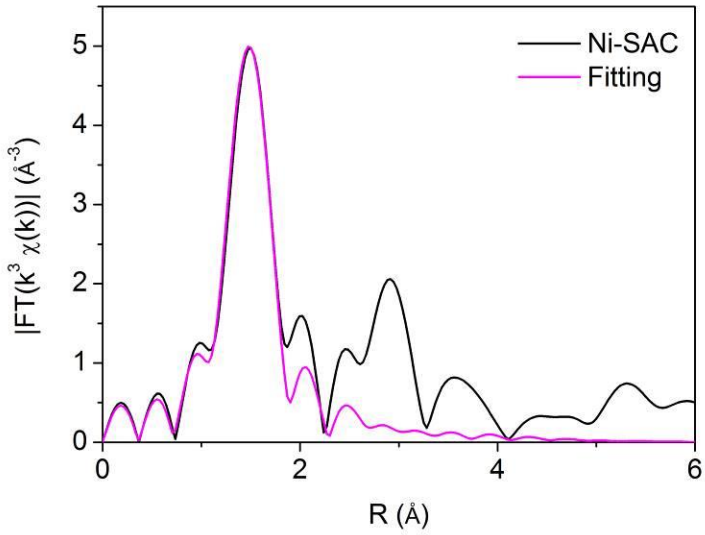

Supplementary Figure 14 | EXAFS fitting result for Ni-SAC. Ni K-edge EXAFS (R space plot) for Ni-SAC.

Supplementary Figure 14 confirms that Ni atoms in Ni-SAC were coordinated four fold by N atoms.

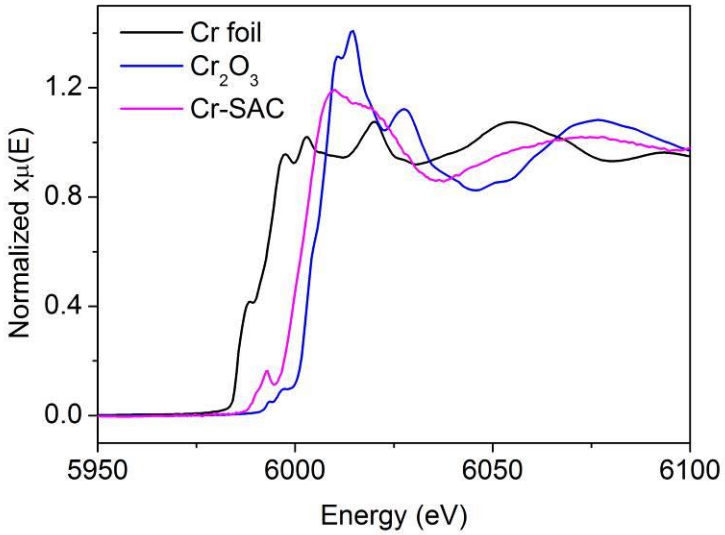

Supplementary Figure 15 | The oxidation state of Cr in Cr-SAC. Cr K-edge XANES spectra for Cr-SAC and different chromium reference materials.

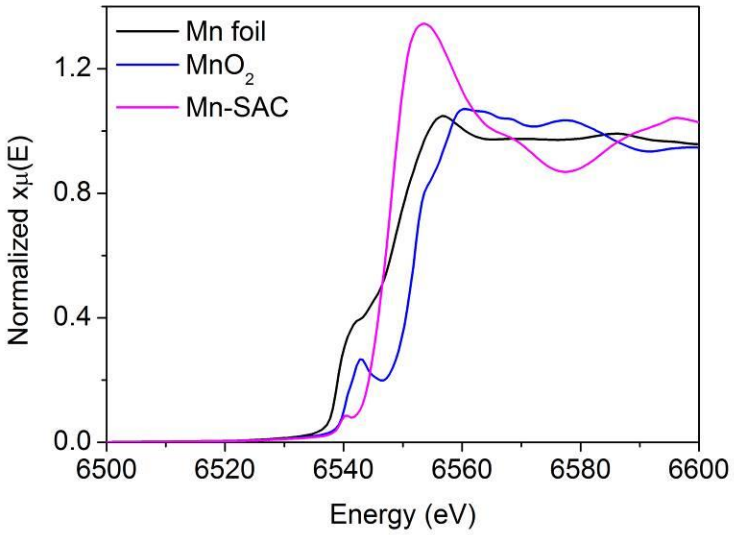

Supplementary Figure 16 | The oxidation state of Mn in Mn-SAC. Mn K-edge XANES spectra for Mn-SAC and a manganese foil reference.

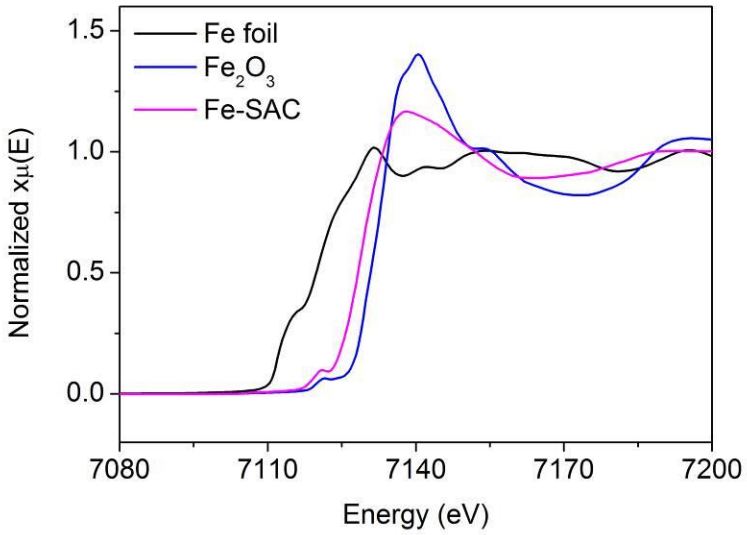

Supplementary Figure 17 | The oxidation state of Fe in Fe-SAC. Fe K-edge XANES spectra for Fe-SAC and different iron reference materials.

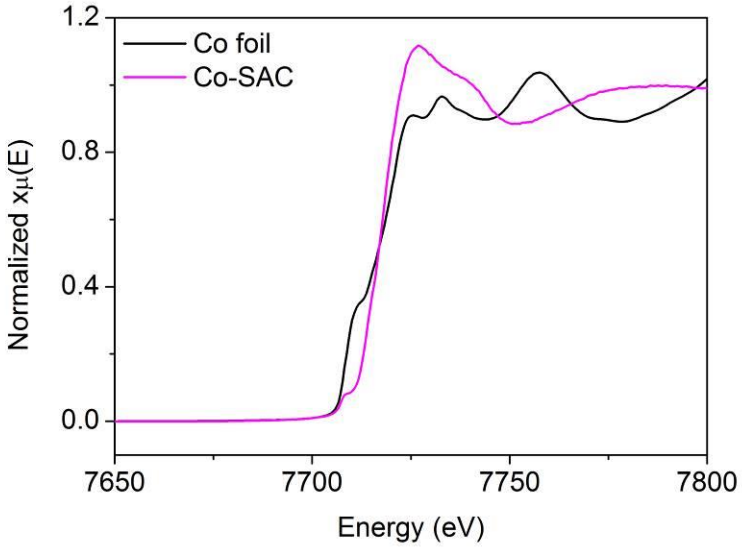

Supplementary Figure 18 | The oxidation state of Co in Co-SAC. Co K-edge XANES spectra for Co-SAC and a cobalt foil reference.

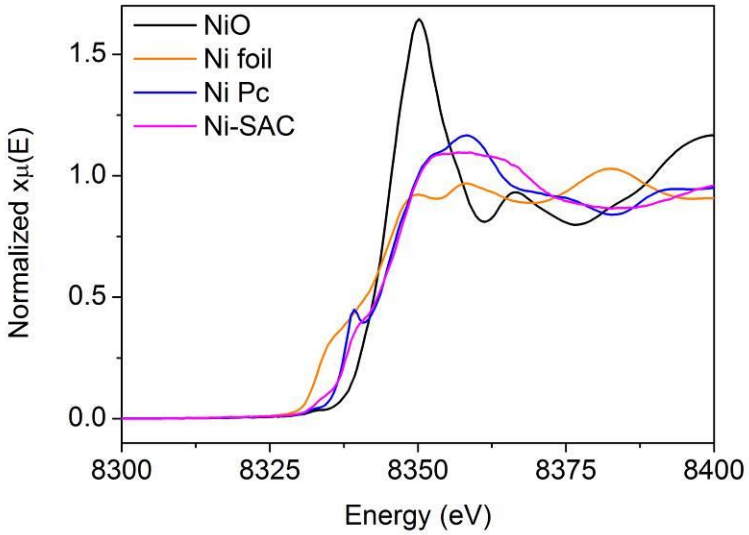

Supplementary Figure 19 | The oxidation state of Ni in Ni-SAC. Ni K-edge XANES spectra for Ni-SAC and different nickel reference materials. Ni-SAC was obtained by heating the Ni precursor (Ni Pc) at 600 ^{o}C for 2 h under an Ar atmosphere.

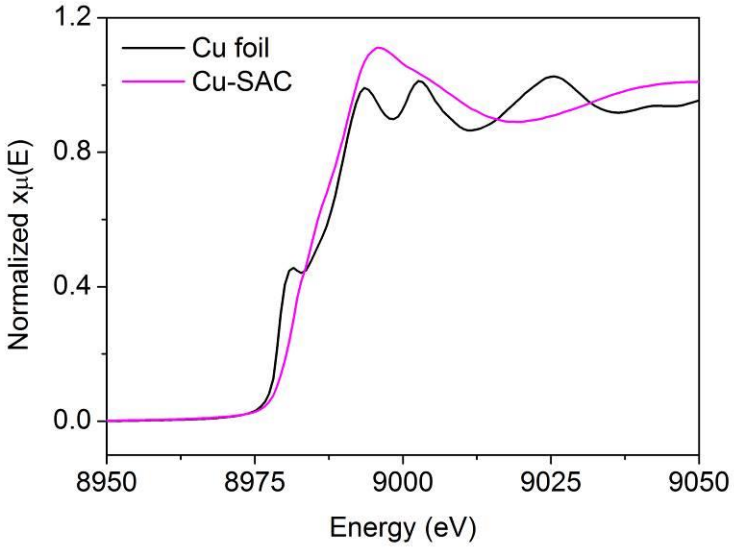

Supplementary Figure 20 | The oxidation state of Cu in Cu-SAC. Cu K-edge XANES spectra for Cu-SAC and a copper foil reference.

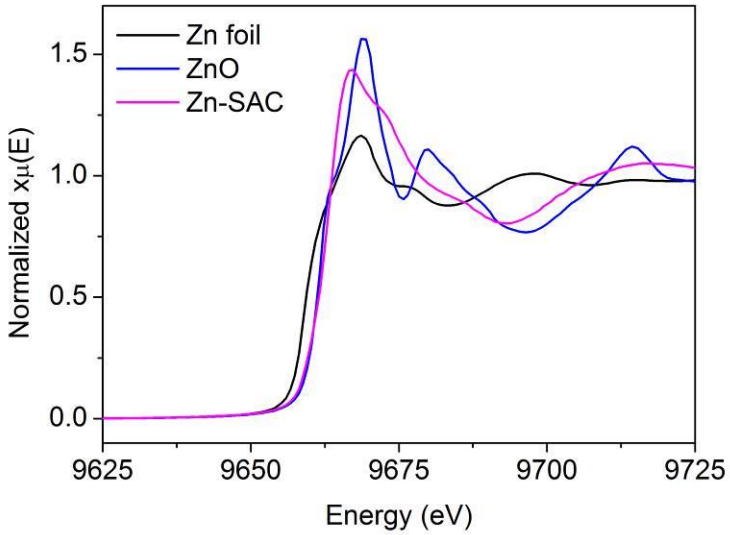

Supplementary Figure 21 | The oxidation state of Zn in Zn-SAC. Zn K-edge XANES spectra for Zn-SAC and different zinc reference materials.

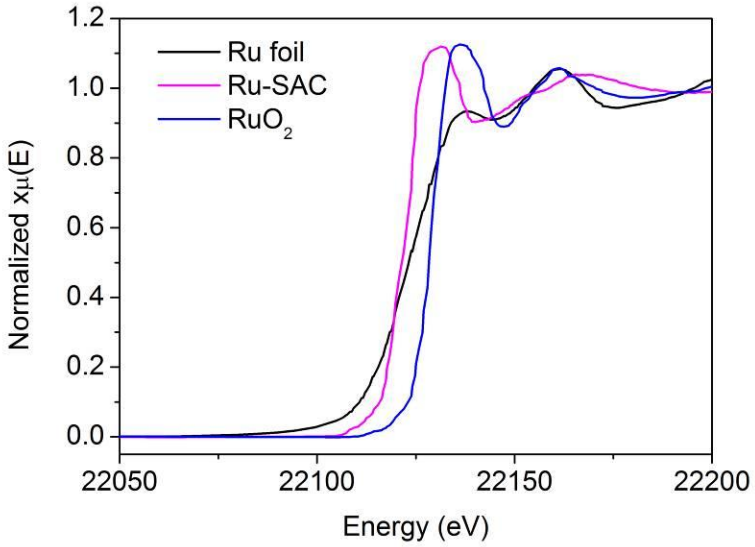

Supplementary Figure 22 | The oxidation state of Ru in Ru-SAC. Ru K-edge XANES spectra for Ru-SAC and different ruthenium reference materials.

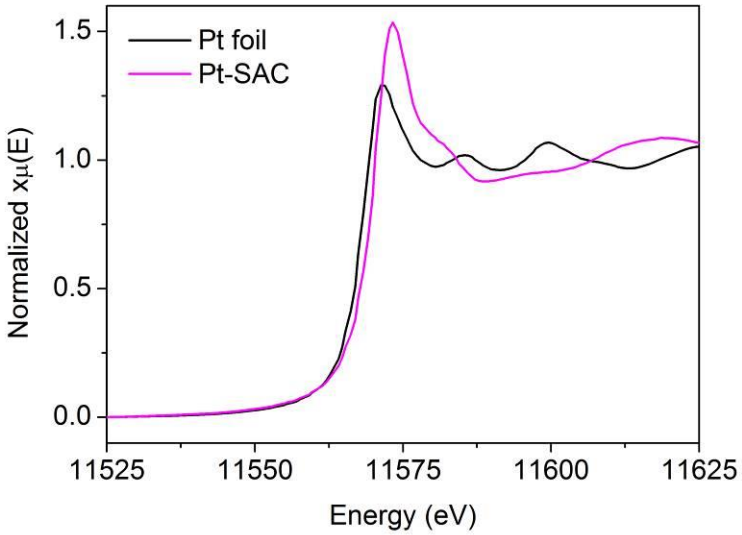

Supplementary Figure 23 | The oxidation state of Pt in Pt-SAC. Pt K-edge XANES spectra for Pt-SAC and a platinum foil reference.

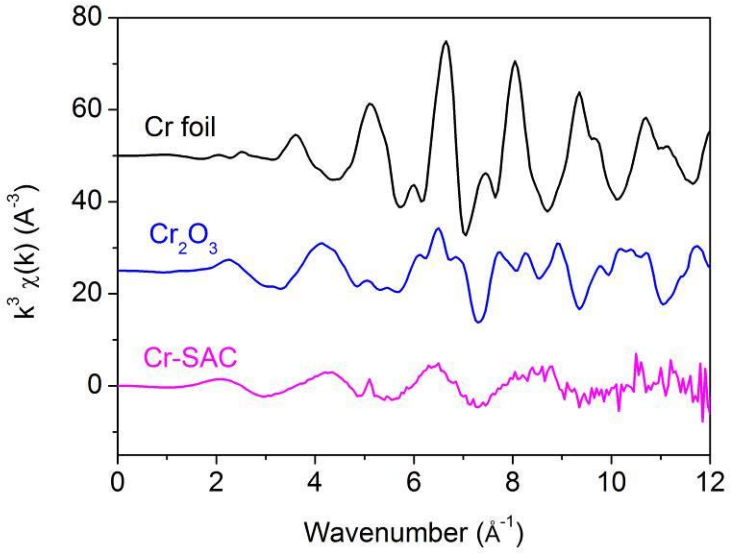

Supplementary Figure 24 | The structure of Cr-SAC. Cr K-edge EXAFS (k space plots) for Cr-SAC and different chromium reference materials.

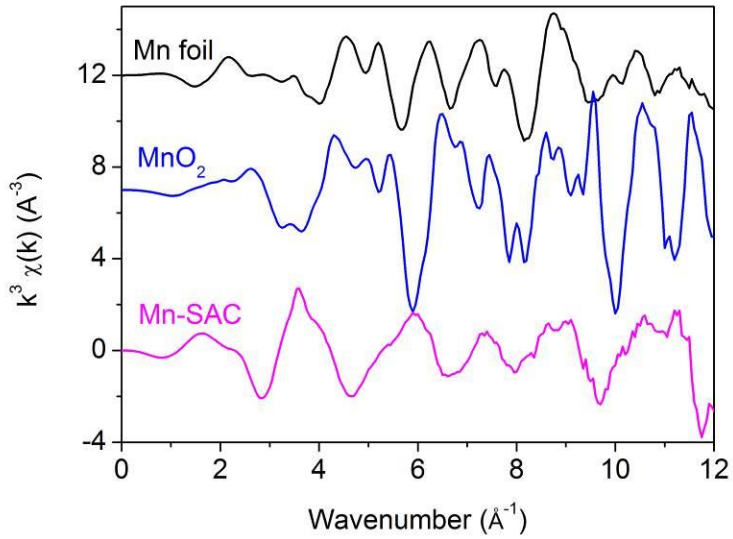

Supplementary Figure 25 | The structure of Mn-SAC. Mn K-edge EXAFS (k space plots) for Mn-SAC and a manganese foil reference.

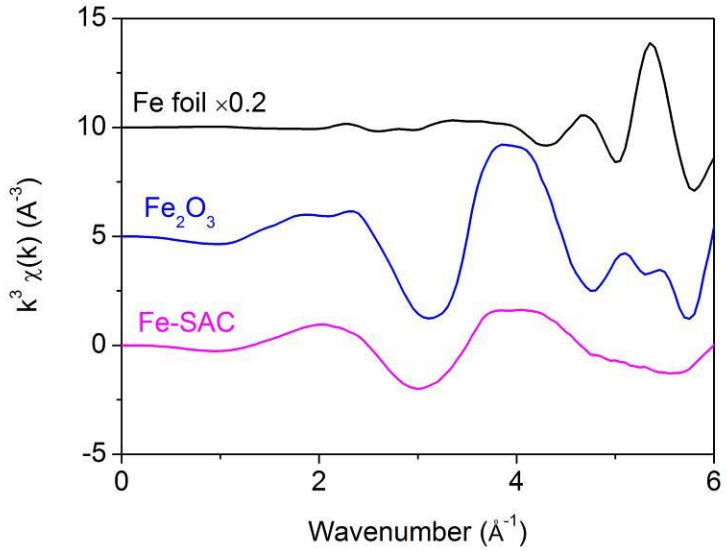

Supplementary Figure 26 | The structure of Fe-SAC. Fe K-edge EXAFS (k space plots) for Fe-SAC and different iron reference materials.

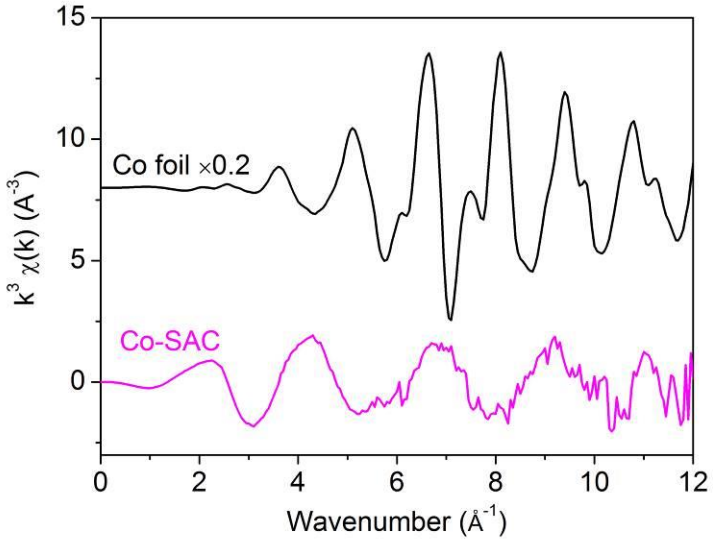

Supplementary Figure 27 | The structure of Co-SAC. Co K-edge EXAFS (k space plots) for Co-SAC and a cobalt foil reference.

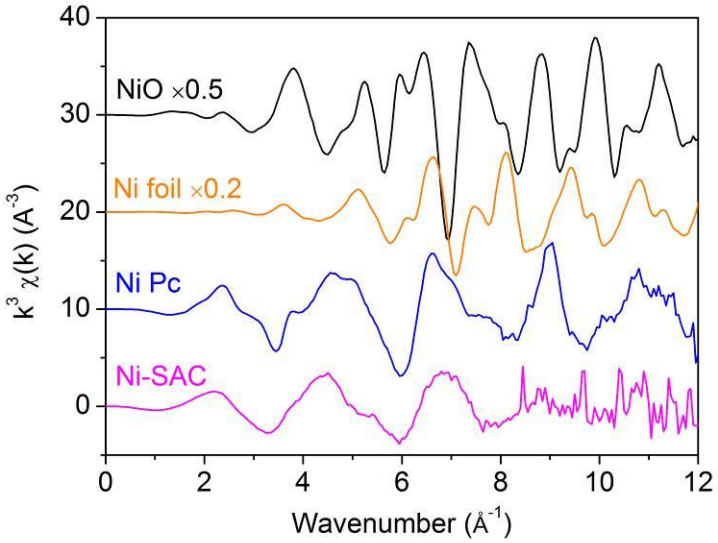

Supplementary Figure 28 | The structure of Ni-SAC. Ni K-edge EXAFS (k space plots) for Ni-SAC and different nickel reference materials

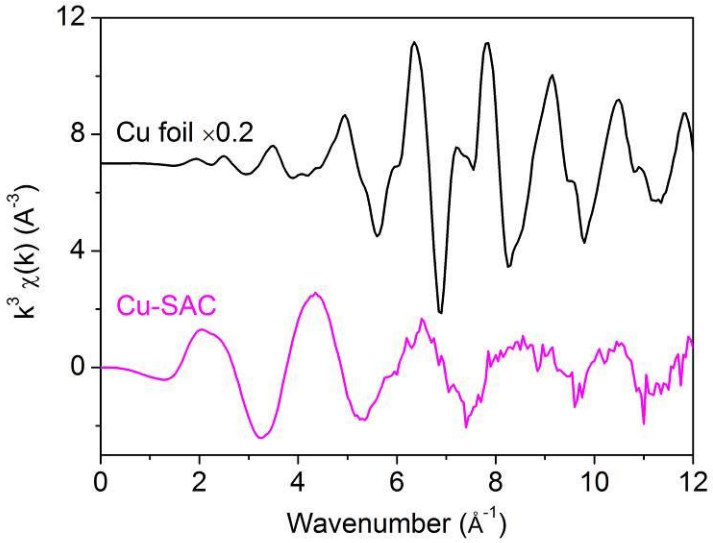

Supplementary Figure 29 | The structure of Cu-SAC. Cu K-edge EXAFS (k space plots) for Cu-SAC and a copper foil reference.

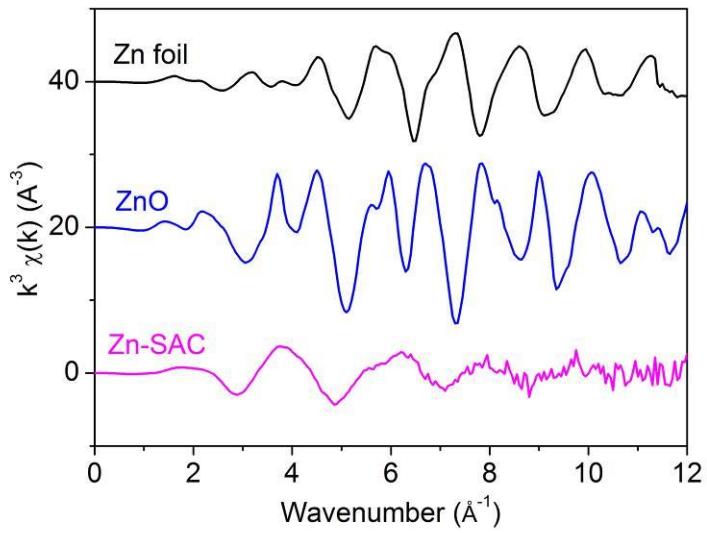

Supplementary Figure 30 | The structure of Zn-SAC. Zn K-edge EXAFS (k space plots) for Zn-SAC and different zinc reference materials.

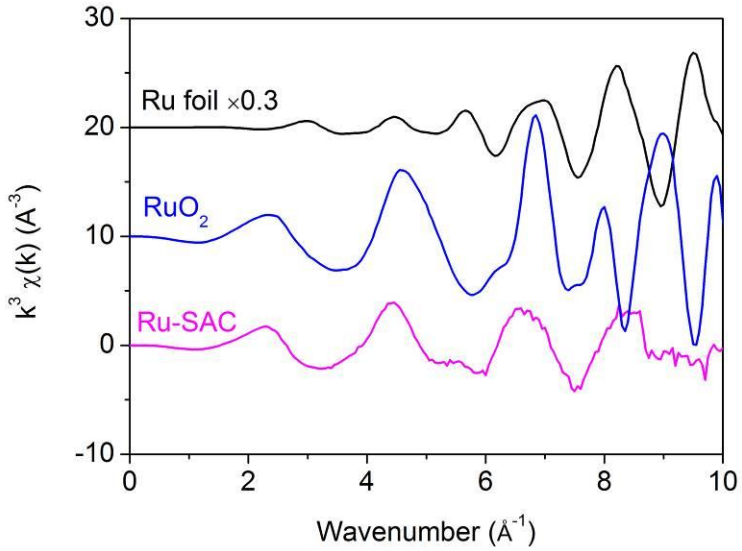

Supplementary Figure 31 | The structure of Ru-SAC. Ru K-edge EXAFS (k space plots) for Ru-SAC and different ruthenium reference materials.

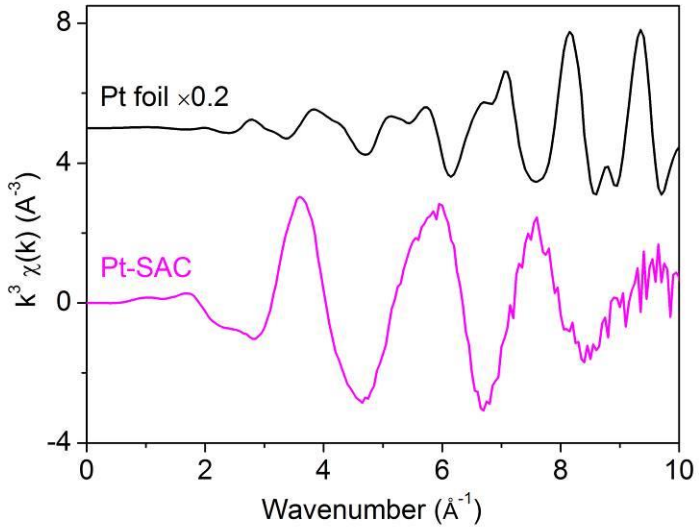

Supplementary Figure 32 | The structure of Pt-SAC. Pt K-edge EXAFS (k space plots) for Pt-SAC and a platinum foil reference.

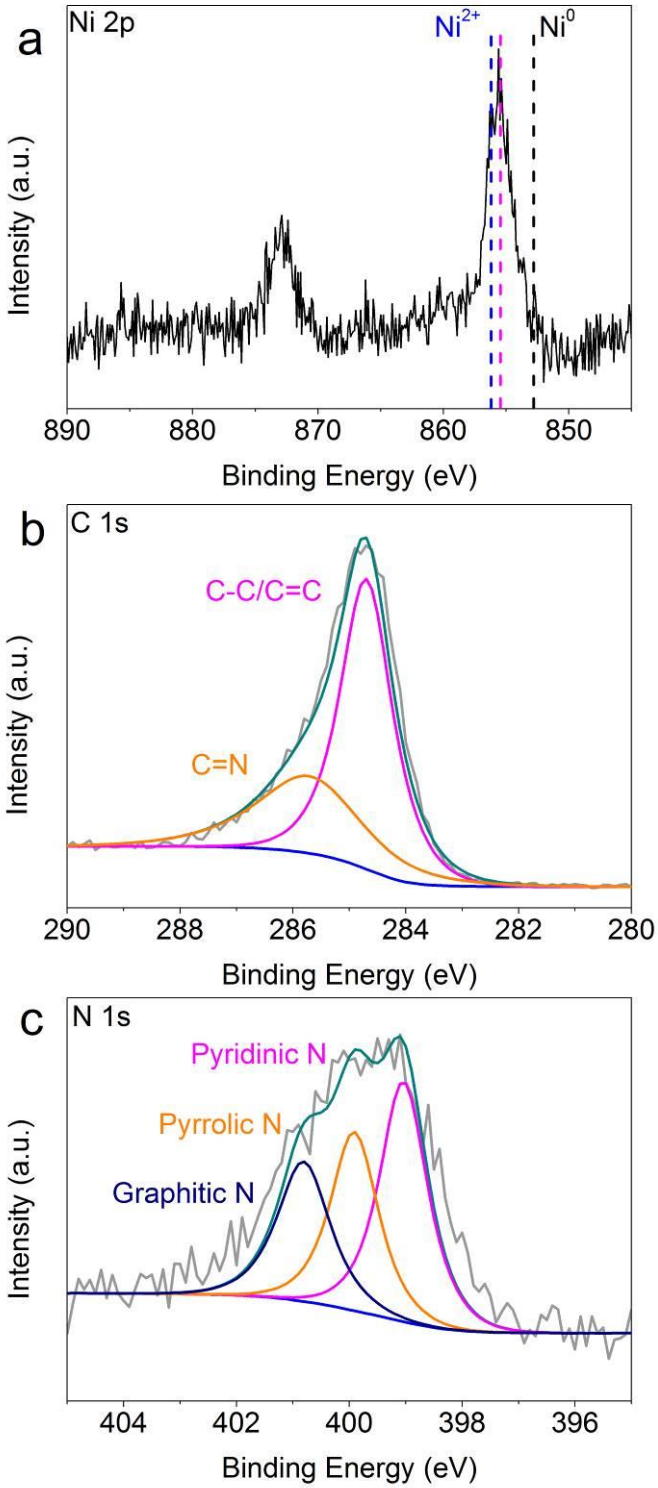

Supplementary Figure 33 | XPS spectra for Ni-SAC. a) Ni 2p region; b) C 1s region; c) N 1s region.

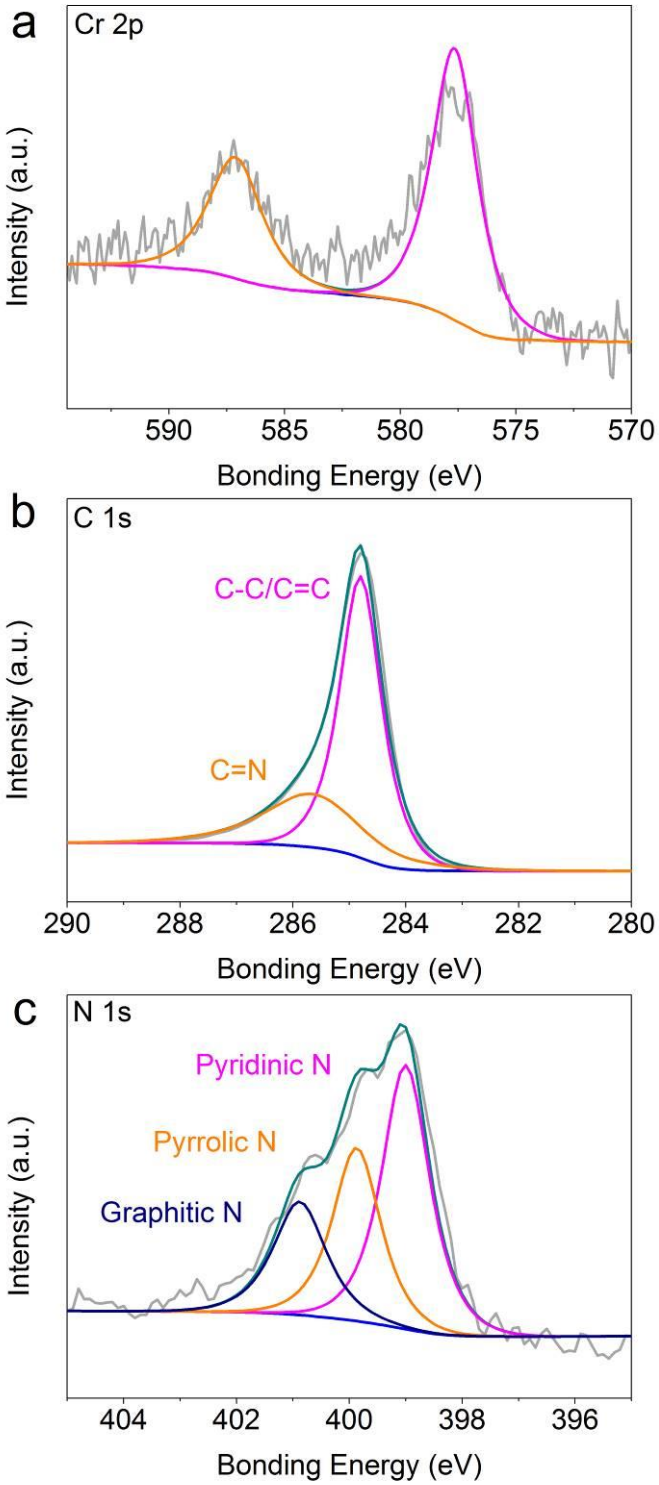

Supplementary Figure 34 | XPS spectra for Cr-SAC. a) Cr 2p region; b) C 1s region; c) N 1s region.

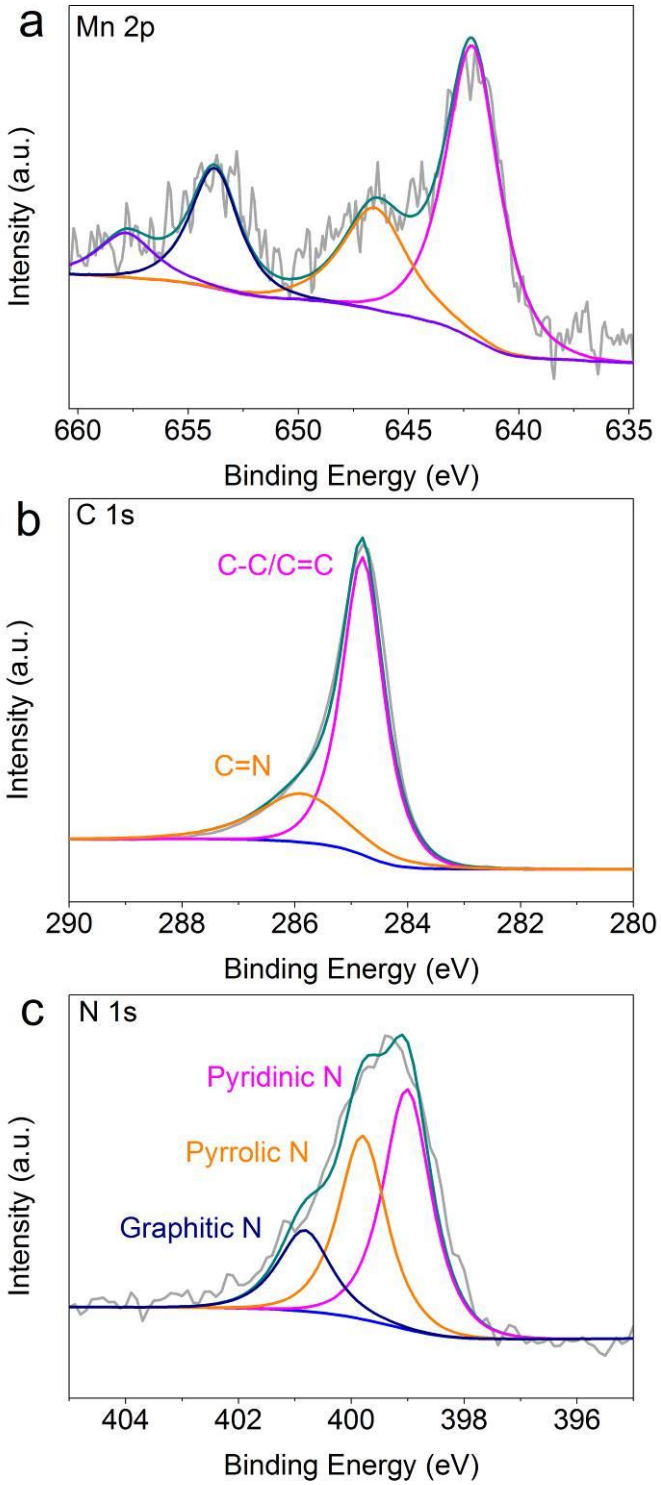

Supplementary Figure 35 | XPS spectra for Mn-SAC. a) Mn 2p region; b) C 1s region; c) N 1s region.

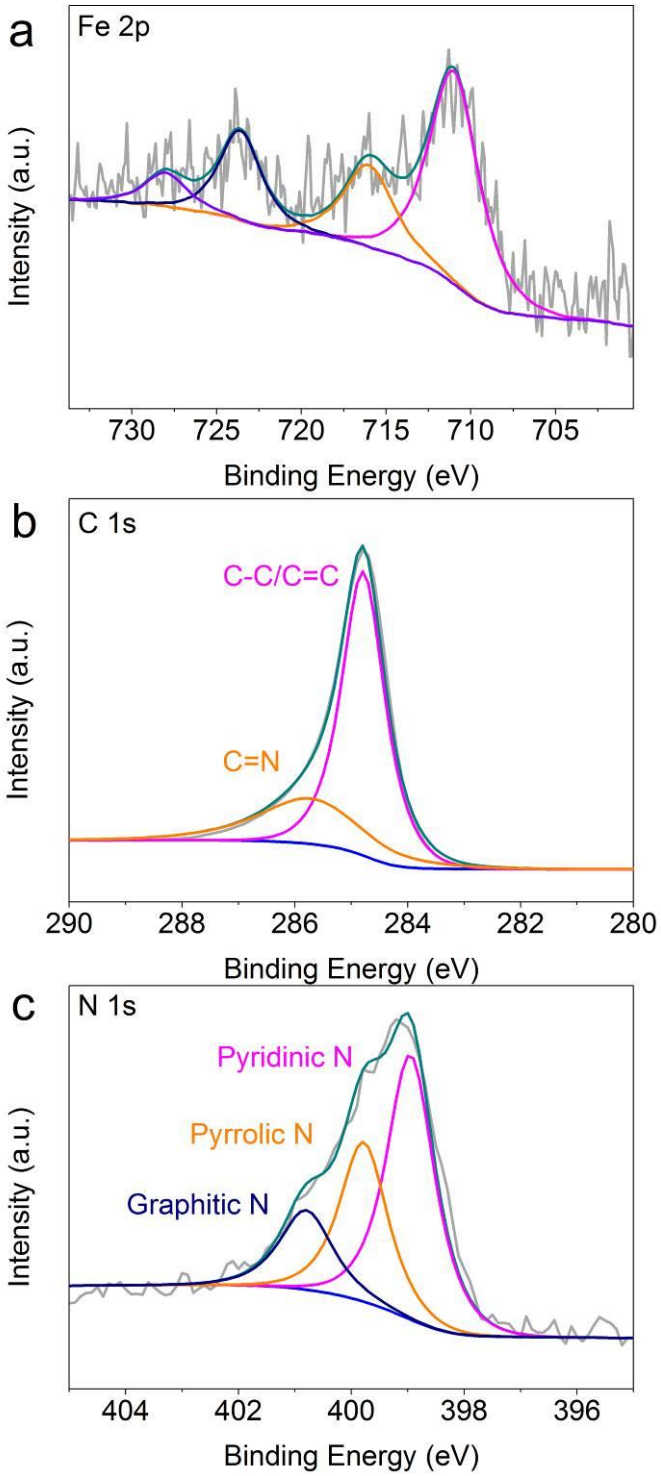

Supplementary Figure 36 | XPS spectra for Fe-SAC. a) Fe 2p region; b) C 1s region; c) N 1s region.

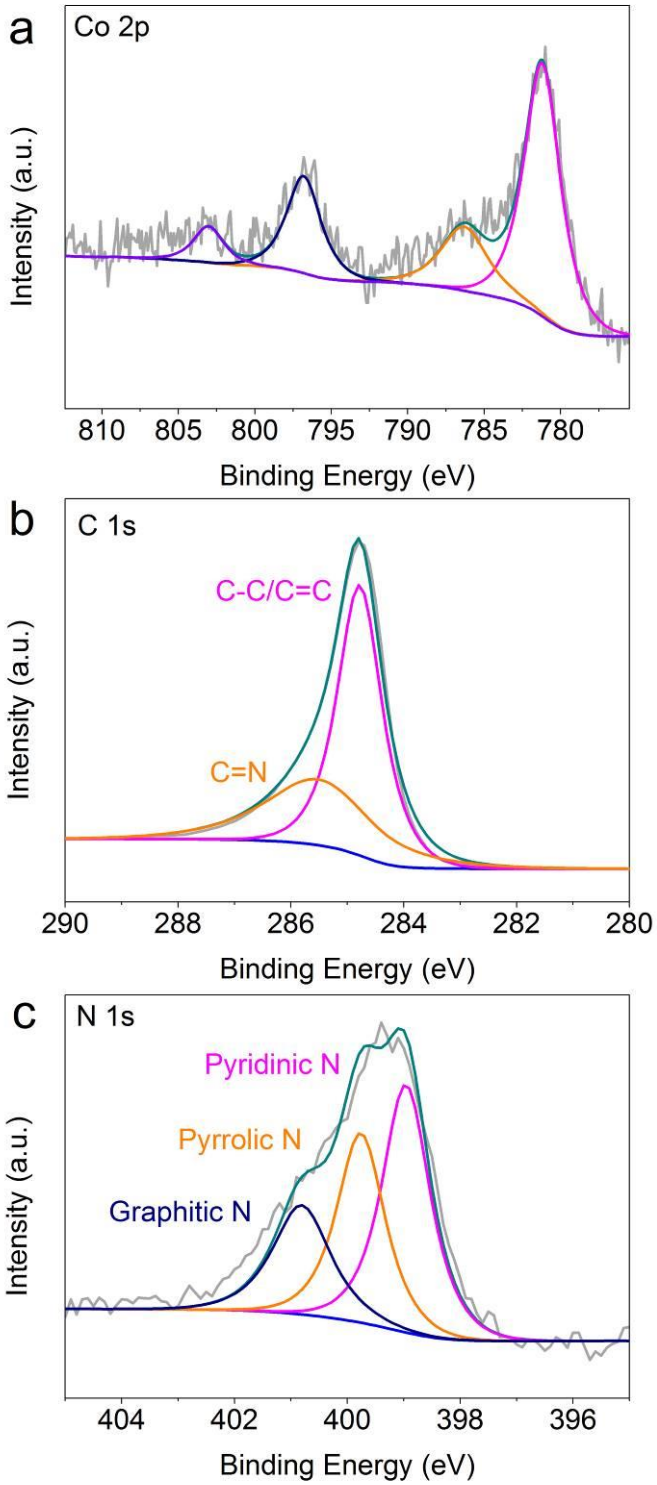

Supplementary Figure 37 | XPS spectra for Co-SAC. a) Co 2p region; b) C 1s region; c) N 1s region.

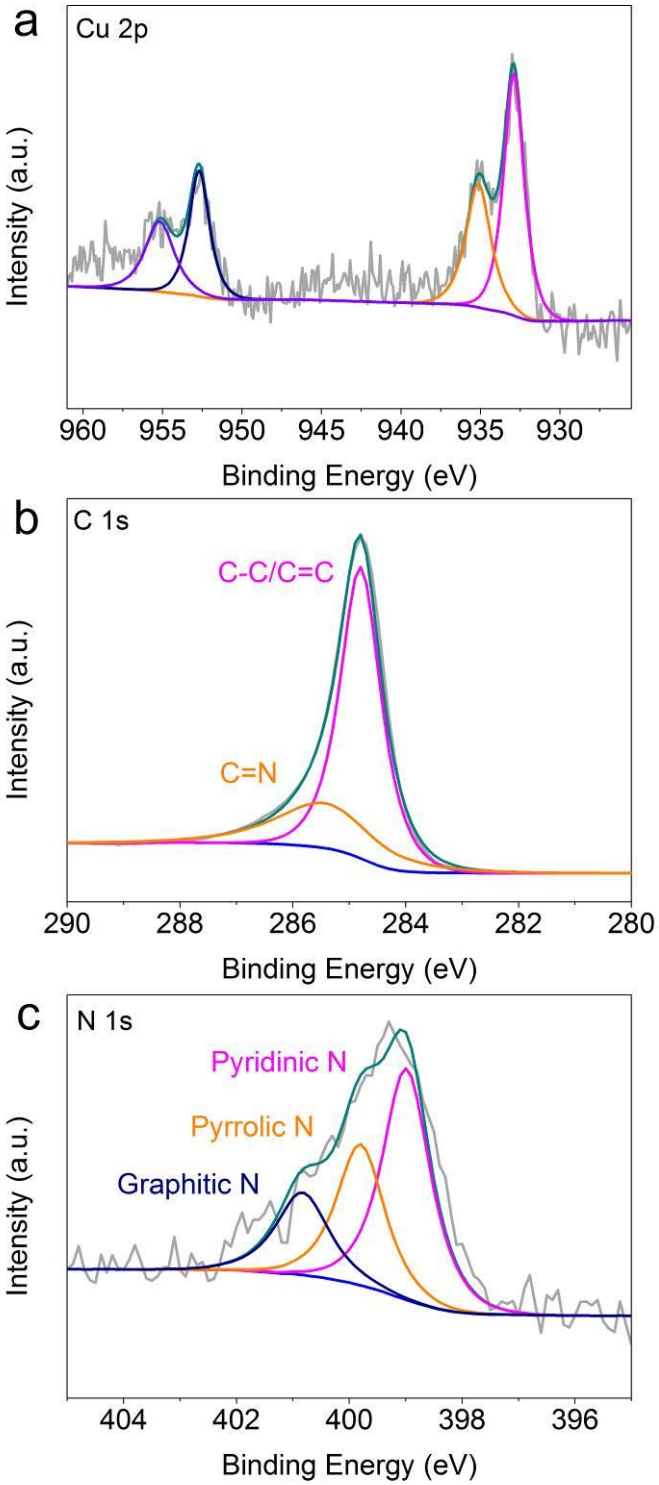

Supplementary Figure 38 | XPS spectra for Cu-SAC. a) Cu 2p region; b) C 1s region; c) N 1s region.

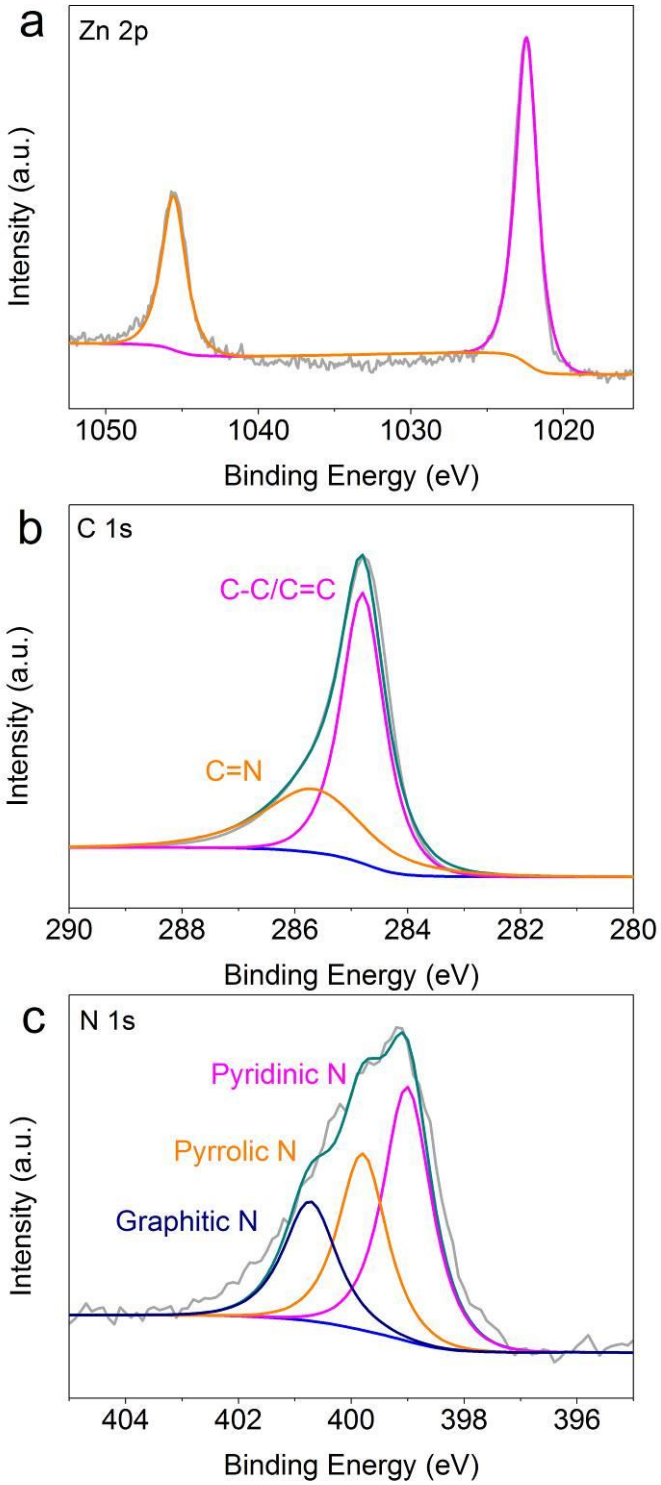

Supplementary Figure 39 | XPS spectra for Zn-SAC. a) Zn 2p region; b) C 1s region; c) N 1s region.

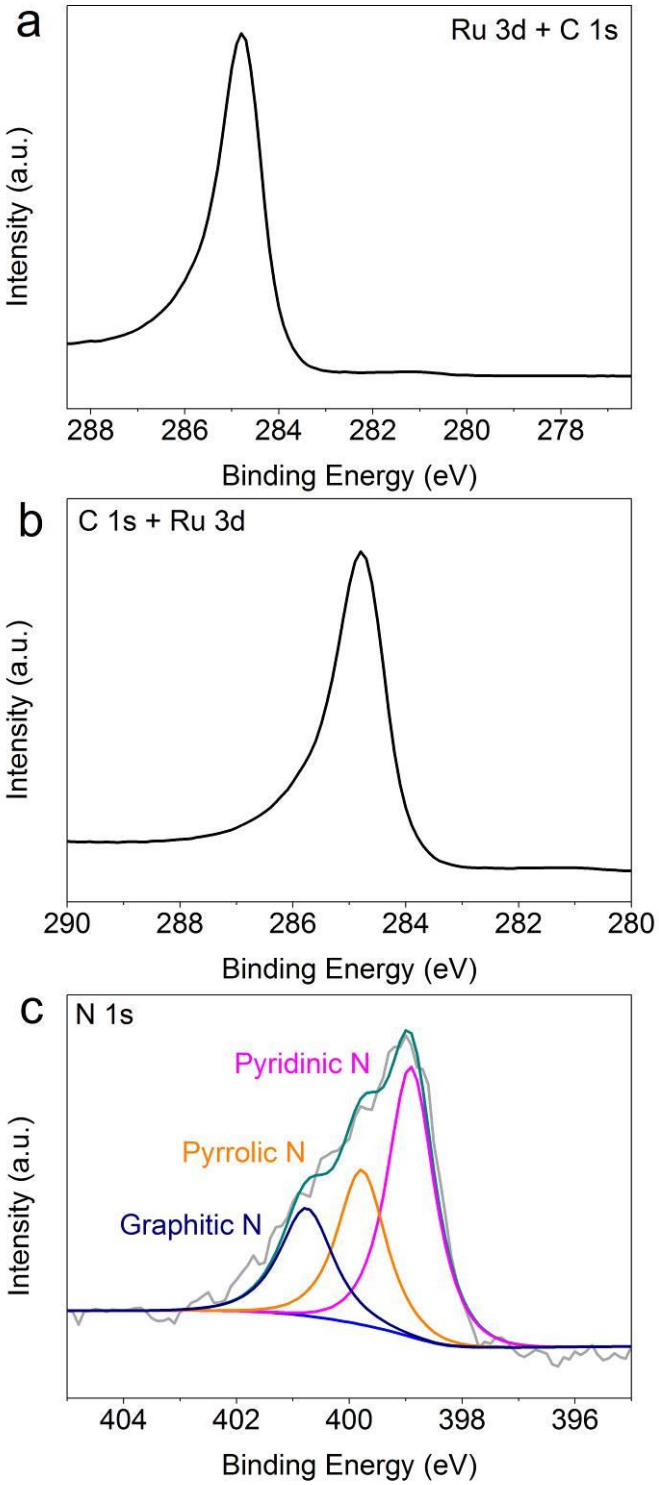

Supplementary Figure 40 | XPS spectra for Ru-SAC. a) Ru 3d region; b) C 1s region; c) N 1s region.

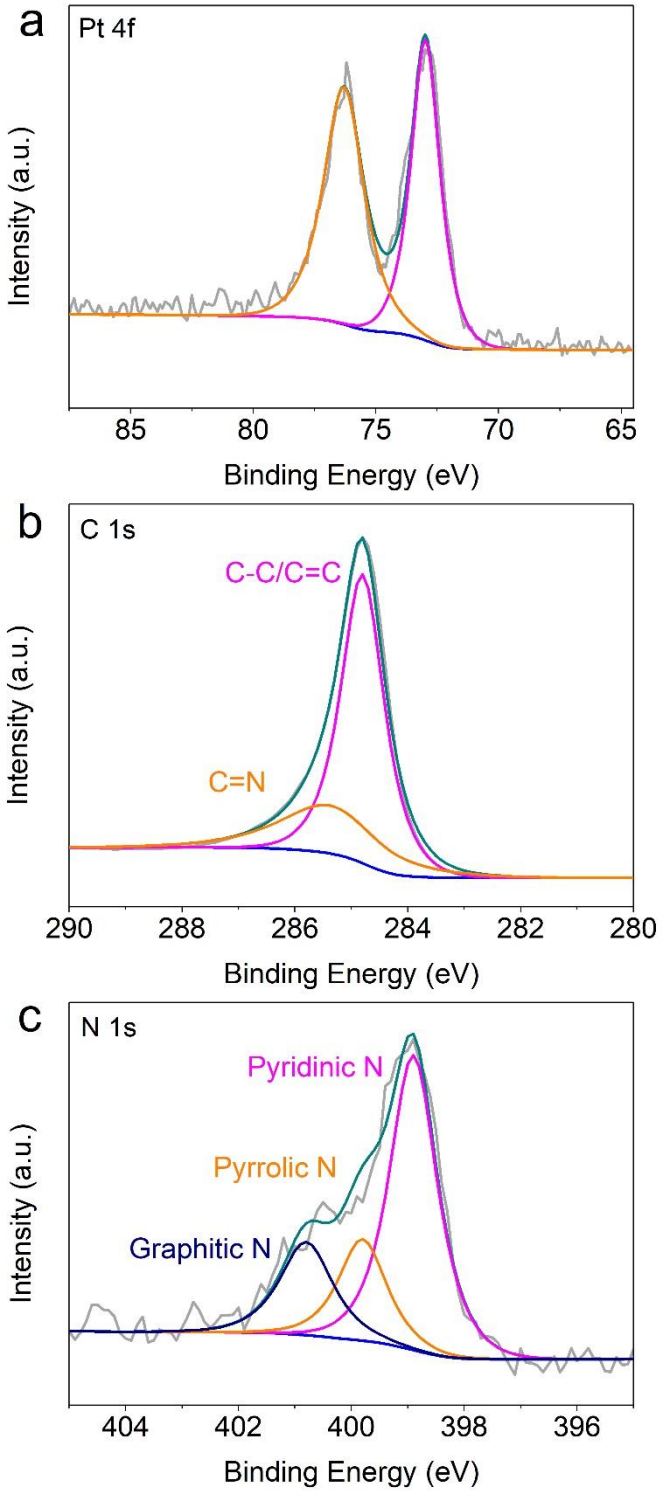

Supplementary Figure 41 | XPS spectra for Pt-SAC. a) Pt 4f region; b) C 1s region; c) N 1s region.

Supplementary Figure 33c indicates that the binding energy of the Ni $2p_{3/2}$ peak was 855.6 eV, higher than that observed for Ni^0 (852.8 eV)[1] and lower than that for Ni^{2+} in NiO (856.2 eV).[2] The data suggest the presence of Ni^{2+} in the N-SAC, with the lower binding energy reflecting Ni^{2+} bonding to less electronegative nitrogen rather than

oxygen. Supplementary Figures 33-41 confirm that all the other M-SACs contain M^{2+} cations. The C 1s spectra were deconvoluted into neutral carbon (i.e. C-C/C=C) and C-N species. The N 1s spectra were deconvoluted into pyridinic-N, pyrrolic-N, and graphitic-N species.[3]

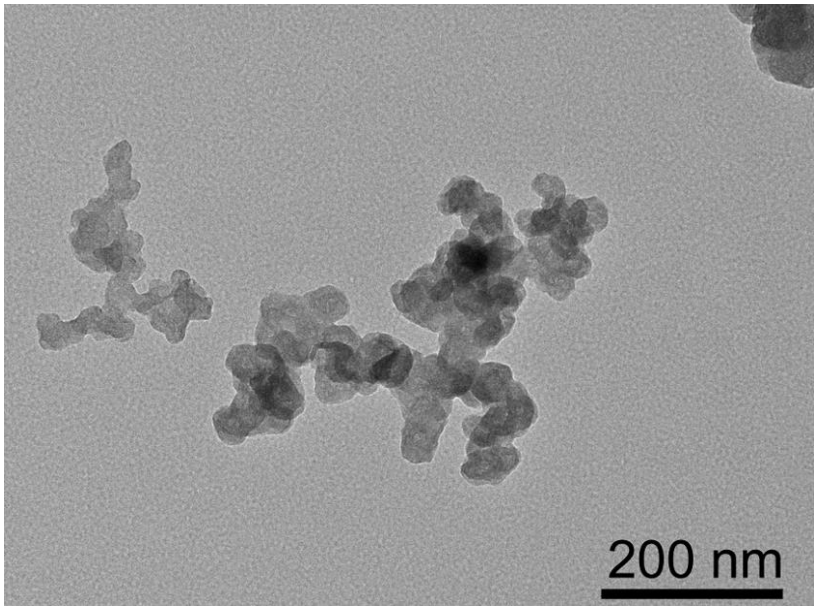

Supplementary Figure 42 | Morphology of Ni-SAC-2.5. TEM image of Ni-SAC-2.5.

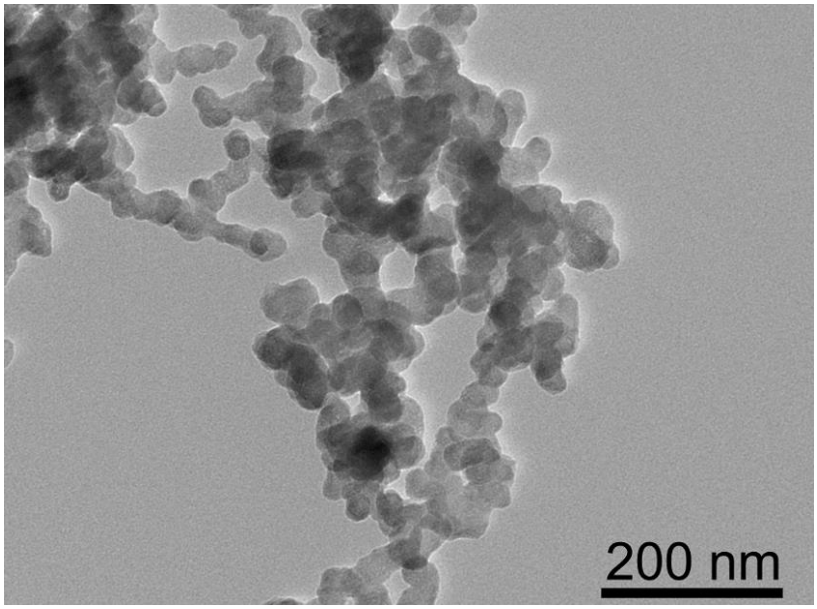

Supplementary Figure 43 | Morphology of Ni-SAC-3.4. TEM image of Ni-SAC-3.4.

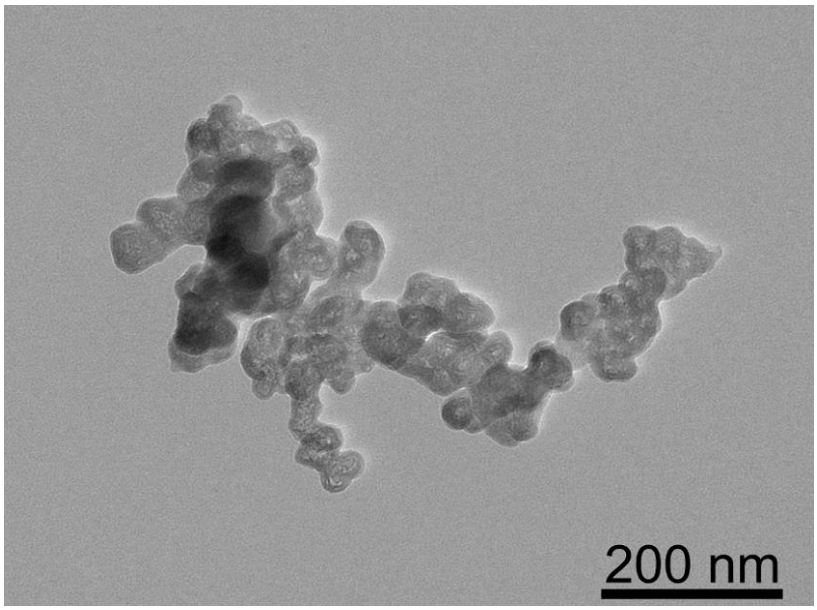

Supplementary Figure 44 | Morphology of Ni-SAC-4.5. TEM image of Ni-SAC-4.5.

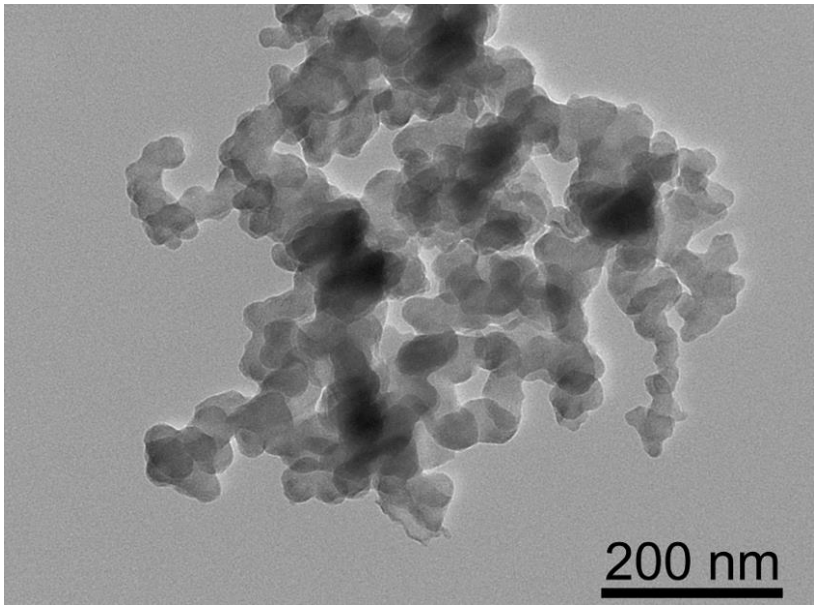

Supplementary Figure 45 | Morphology of Ni-SAC-5.3. TEM image of Ni-SAC-5.3.

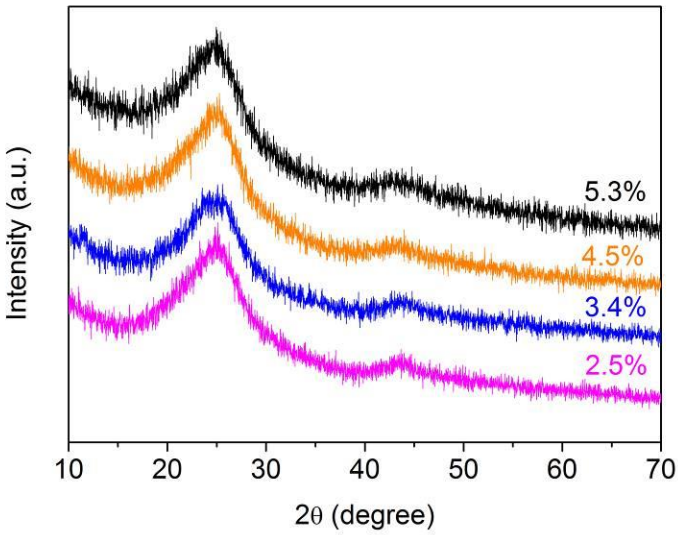

Supplementary Figure 46 | Characterization of Ni-SACs with different metal loadings. XRD patterns for Ni-SAC-*x* at different Ni loadings.

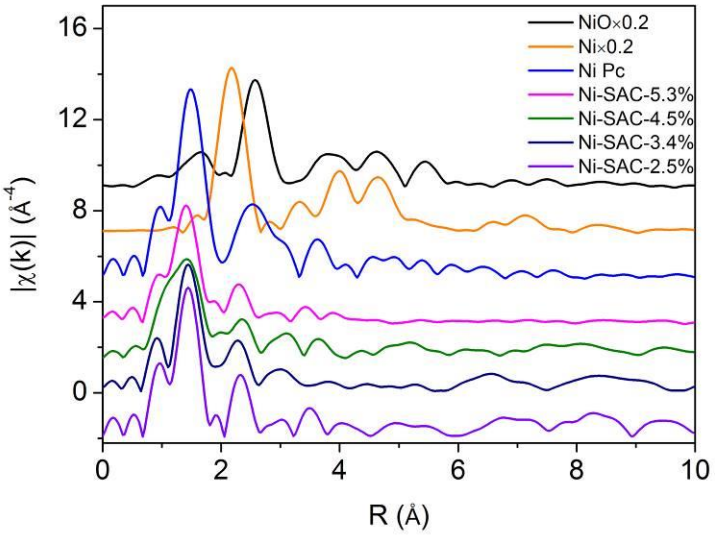

Supplementary Figure 47 | The structure of Ni-SACs with different metal loadings. Ni K-edge EXAFS (R space plots) for Ni-SAC-*x* at different Ni loadings.

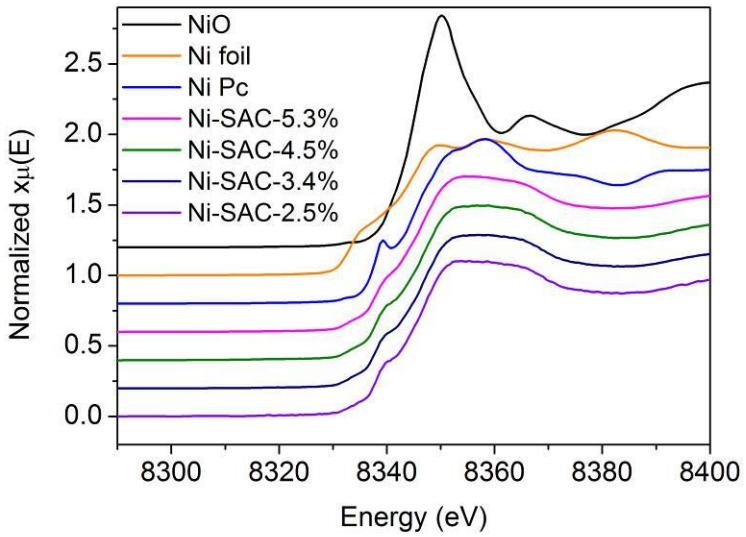

Supplementary Figure 48 | The oxidation state of Ni in Ni-SACs with different metal loadings. Ni K-edge XANES spectra for Ni-SAC-*x* with different Ni loadings.

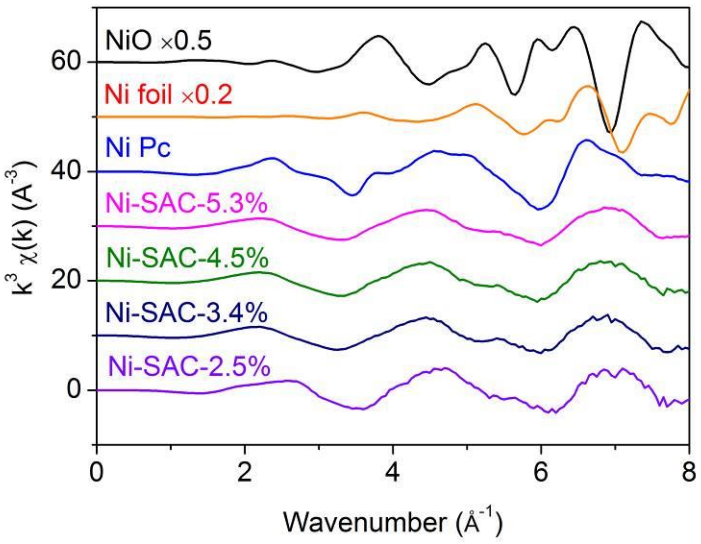

Supplementary Figure 49 | The structure of Ni-SACs with different metal loadings. Ni K-edge EXAFS (k space plots) for Ni-SAC-*x* at different Ni loadings.

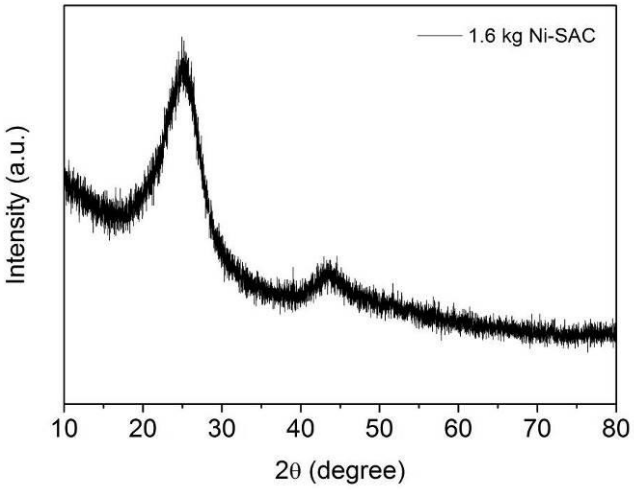

Supplementary Figure 50 | XRD pattern of Ni-SAC synthesized on a large scale.

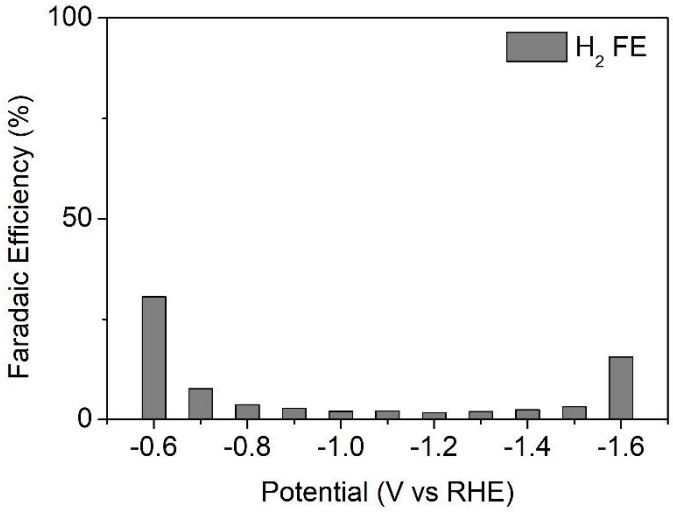

Supplementary Figure 51 | Faradaic efficiency of H_2 for Ni-SAC-2.5 at different potentials.

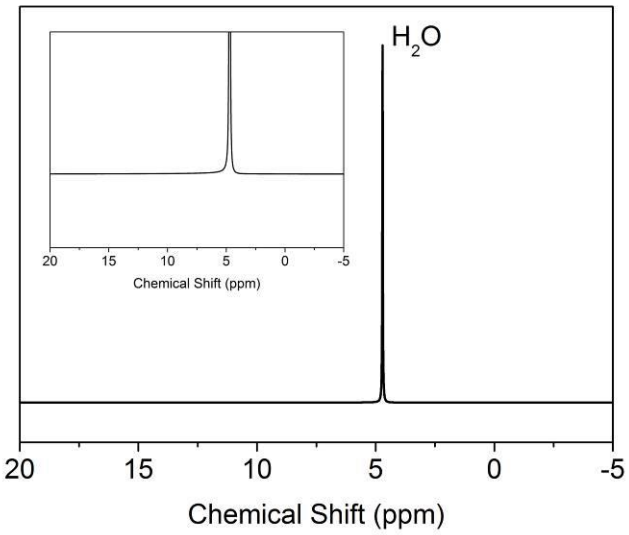

Supplementary Figure 52 | NMR spectrum of liquid products after CO_2RR. No liquid products were detected.

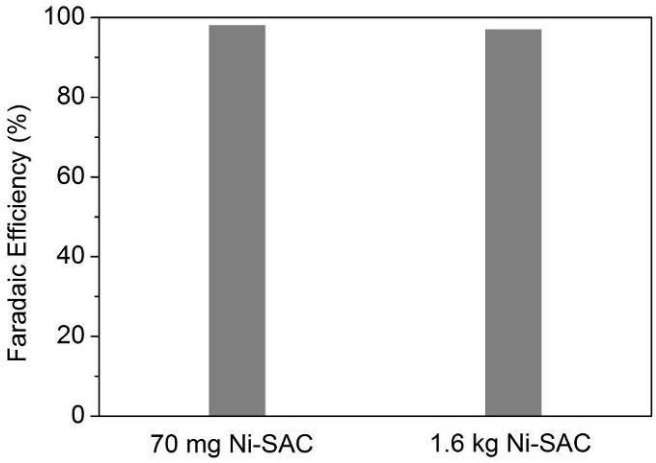

Supplementary Figure 53 | The CO_2RR performance of Ni-SAC synthesized on a large scale. CO_2RR activity of Ni SACs synthesized on a scale of 70 mg and on a scale of 1.6 kg.

Supplementary Figure 53 confirms that the Ni-SAC synthesized on a large scale (1.6 kg) had a very similar CO_2RR performance as Ni-SAC synthesized on a 70 mg scale, indicating that the samples were comparable in performance and that the universal M-SAC synthesis route introduced here was highly scalable.[4,5]

Supplementary Table 1 | Compositional analysis of the different M-SACs. The metal loading, total N content and N speciation of the different M-SACs is indicated.

Sample	Metal loading wt.% (ICP)	Total N content at.% (XPS)	Pyridinic N content at.%	Pyrolic N content at.%	Graphitic N content at.%
Cr-SAC	3.58	3.34	1.63	1.01	0.70
Mn-SAC	2.30	2.43	1.14	0.87	0.42
Fe-SAC	1.85	2.32	1.20	0.72	0.40
Co-SAC	2.97	3.26	1.42	1.09	0.75
Ni-SAC	5.32	6.75	3.42	1.93	1.40
Cu-SAC	2.59	3.4	1.71	0.87	0.82
Zn-SAC	3.65	3.55	1.61	1.11	0.83
Ru-SAC	2.67	2.12	1.04	0.61	0.47
Pt-SAC	2.16	1.57	0.93	0.32	0.32

Supplementary Table 2 | Metal loading comparison with other reported Ni-SAC materials

Sample	Metal loading	Measurement method	Reference
Ni-SAC@graphene	0.05 at.%	ICP	*6*
Ni-SAC@commercial carbon	0.27 wt.%	ICP	*7*
Ni-SAC@MOF	0.31 wt.%	ICP	*4*
Ni-SAC@g-C_3N_4	1.41 wt.%	ICP	*8*
Ni-SAC@MOF	1.53 wt.%	ICP	*5*
Ni-SAC@graphene oxide	0.44 at.%	XPS	*9*
Ni-SAC@g-C_3N_4	4.6 wt.%	ICP	*10*
Ni-SAC@commercial carbon	5.32 wt.%	ICP	**This work**

Supplementary References

1 Mansour, A. N. Nickel Monochromated Al Kα XPS Spectra from the Physical Electronics Model 5400 Spectrometer. *Surf. Sci. Spectra* **3**, 221-230 (1994).

2 Mansour, A. N. Characterization of NiO by XPS. *Surf. Sci. Spectra* **3**, 231-238 (1994).

3 Cao, Y., Mao, S., Li, M., Chen, Y. & Wang, Y. Metal/Porous Carbon Composites for Heterogeneous Catalysis: Old Catalysts with Improved Performance Promoted by N-Doping. *ACS Catal.* **7**, 8090-8112 (2017).

4 Yunteng Qu *et al.* Direct Transformation of Bulk Copper into Copper Single Sites via Emitting and Trapping of Atoms. *Nat. Catal.* **1**, 781-786 (2018).

5 Zhao, C. *et al.* Ionic Exchange of Metal-Organic Frameworks to Access Single Nickel Sites for Efficient Electroreduction of CO_2. *J. Am. Chem. Soc.* **139**, 8078-8081 (2017).

6 Fei, H. *et al.* General Synthesis and Definitive Structural Identification of MN_4C_4 Single-Atom Catalysts with Tunable Electrocatalytic Activities. *Nat. Catal.* **1**, 63-72 (2018).

7 Zheng, T. *et al.* Large-Scale and Highly Selective CO_2 Electrocatalytic Reduction on Nickel Single-Atom Catalyst. *Joule* **3**, 265-278 (2019).

8 Li, X. *et al.* Exclusive Ni-N_4 Sites Realize Near-Unity CO Selectivity for Electrochemical CO_2 Reduction. *J. Am. Chem. Soc.* **139**, 14889-14892 (2017).

9 Jiang, K. *et al.* Isolated Ni Single Atoms in Graphene Nanosheets for High-performance CO_2 Reduction. *Energy Environ. Sci.* **11**, 893-903 (2018).

10 Yang, H. B. *et al.* Atomically Dispersed Ni(i) as the Active Site for Electrochemical CO_2 Reduction. *Nat. Energy* **3**, 140-147 (2018).